International Journal of Chemical, Materials and Biomolecular Sciences
ISSN: 2415-6620
Vol:13, No:5, 2019

Feasibility Study of Friction Stir Welding Application for Kevlar Material

Ahmet Taşan, Süha Tirkeş, Yavuz Öztürk, Zafer Bingül

***Abstract*—**Friction stir welding (FSW) is a joining process in the solid state, which eliminates problems associated with the material melting and solidification, such as cracks, residual stresses and distortions generated during conventional welding. Among the most important advantages of FSW are; easy automation, less distortion, lower residual stress and good mechanical properties in the joining region. FSW is a recent approach to metal joining and although originally intended for aluminum alloys, it is investigated in a variety of metallic materials. The basic concept of FSW is a rotating tool, made of non-consumable material, specially designed with a geometry consisting of a pin and a recess (shoulder). This tool is inserted as spinning on its axis at the adjoining edges of two sheets or plates to be joined and then it travels along the joining path line. The tool rotation axis defines an angle of inclination with which the components to be welded. This angle is used for receiving the material to be processed at the tool base and to promote the gradual forge effect imposed by the shoulder during the passage of the tool. This prevents the material plastic flow at the tool lateral, ensuring weld closure on the back of the pin. In this study, two 4 mm Kevlar® plates which were produced with the Kevlar® fabrics, are analyzed with COMSOL Multiphysics in order to investigate the weldability via FSW. Thereafter, some experimental investigation is done with an appropriate workbench in order to compare them with the analysis results.

***Keywords*—**Analytical modeling, composite materials welding, friction stir welding, heat generation.

I. Introduction

FRICTION stir welding (FSW) is particularly suitable for the non-ferrous metals which have low melting point. Additionally, some compound materials such as aluminum alloys and steels can also be readily welded. During welding, a rotating cylindrical pin is traveled throughout joint line of the materials and resulting from heating the materials to a plasticized state and stirring the workpieces together, a joint is formed.

Thanks to advances in FSW, hardly weldable steels or dissimilar materials such as aluminum, magnesium, copper, and titanium can be welded to each other. This technology is can be applied in many industries such as automotive, aviation, defense and electronics.

Ahmet Taşan is with the TÜBİTAK (The Scientific and Technological Research Council of Turkey), and with the Mechatronic Engineering Department, University of Kocaeli Kocaeli, Turkey (e-mail: ahmet.tasan@tubitak.gov.tr).

Süha Tirkeş is with the Welding Technology and NDT Research/ Application Centre of Middle East Technical University (METU), Ankara, Turkey (e-mail: stirkes@metu.edu.tr)

Yavuz Öztürk is with the Department of Engineering Electrical Engineering Division, University of Cambridge, 9 JJ Thomson Avenue, Cambridge, CB3 0FA United Kingdom (e-mail: yo268@cam.ac.uk).

Zafer Bingül is with the Mechatronic Engineering Department, University of Kocaeli, Kocaeli, Turkey (e-mail:zaferb@kocaeli.edu.tr)

II. Process Review

Fig. 1 shows that the process applies plunge force, torque and traverse force on the workpieces to be welded via a nonconsumable rotating tool with a specially designed pin and shoulder [1].

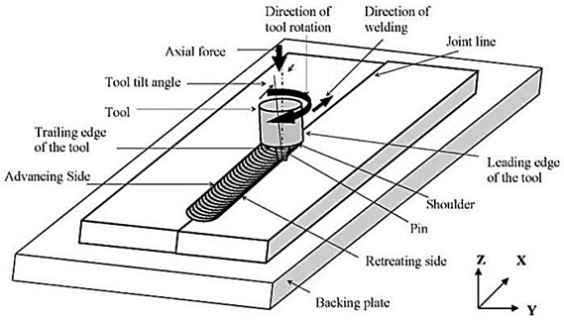

Fig. 1 Schematic drawing of FSW process

Fig. 2 illustrates that along the joint line, two square butt grooved plates without any welding groove preparation can be welded via a tool with a specially designed pin and shoulder under applied specific process parameters such as tilt angle (θ), plunge force (F), rotating speed (ω) and travelling speed (v) [1].

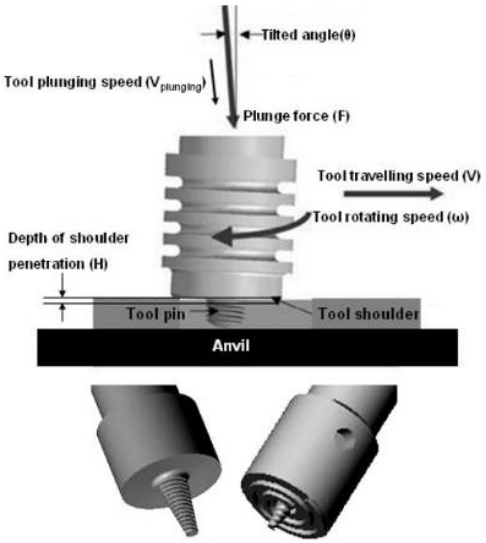

Fig. 2 Schematic of a FSW tool and processing parameters

Compared to fusion welding, some benefits of FSW are summarized as described;

i. No loss of alloying elements.
ii. Dimensional stability and repeatability.
iii. Excellent mechanical properties.
iv. Avoiding porosity and cracks in the welding area.
v. Consumable materials saving such as wire, shielding gas.
vi. Welding compound and alloy steels such as: Al, Ti, Cu, Ni, Mg.
vii. No harmful emissions.
viii. Minimizing grinding wastes.
ix. Reduced weights (40 % less than fusion welds).

According to the literature researches, compared to metal inert gas welding (MIG), FSW is 4 times faster than for 5 mm thick AA6062-T6 and 2 times for 10 mm thick AA6062-T6, as seen in Fig. 3. As mentioned before, the reasons of this time saving are, elimination of welding groove preparation, surface cleaning before and after welding and consumable materials replacement during welding [2].

AA 6082-T6	t = 5 mm	t = 5 mm	t = 10 mm	t = 10 mm
One sided welding	MIG	FSW	MIG	FSW
Preparation	V – groove, 60°	-	-	-
Cleaning with alcohol	-	0,5 min/m	-	0,5 min / m
Brushing prior to welding	2 min / m	-	2 min/m	-
Welding current	200 A	-	200/250 A	-
Shielding gas	Ar	-	Ar	-
Welding speed	0,5 m/ min	2 m/ min	0.6/0,3 m/ min	1,0 m / min
Consumable	OK 18.16 Ø1,2 mm	-	OK 18.16 Ø1,2 mm	-
Number of runs	1	1	1+1	1
Total time / one meter of weld	**4 min**	**1 min**	**7 min**	**1,5 min**

Fig. 3 Time needed to weld 1 meter on AA6062-T6 in FSW and MIG processes

A. Joint Configurations

Among many advantages over to other fusing welding methods, as seen in Fig. 4, FSW also facilitates welding materials with the other joint configurations [3].

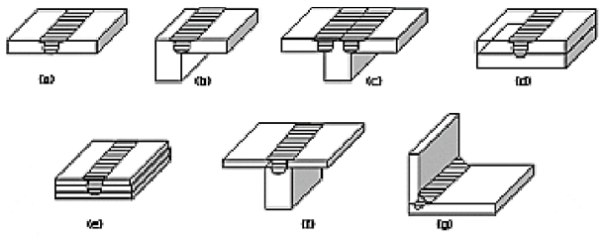

Fig. 4 Possible joint configurations for FSW. (a) Square butt groove, (b) Edge butt groove, (c) T-butt groove, (d) Lap groove, (e) Multiple lap groove, (f) T-lap groove, (g) Fillet groove.

B. Microstructure Zones

Due to the fact that FSW has many variable parameters including plunge force, rotating force, traverse force, tool geometry and material, the microstructure of the process can be changeable. Fig. 5 illustrates the microstructure and regions of FSW which are accepted by TWI [3].

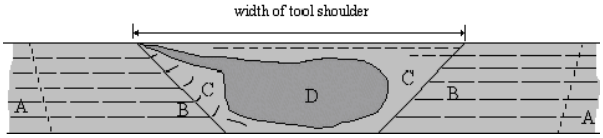

Fig. 5 Schematic of the various microstructure regions of FSW

The microstructure includes distinct regions into the weld zone as follows:

i. *A:* Unaffected parent metal: This region is material that has not been deformed and not affected by the heat in terms of the microstructure or mechanical properties.
ii. *B:* Heat affected zone (HAZ): This is the region that is closer to the weld-center, although the mechanical properties or the microstructure has been modified, there is no plastic deformation occurring in this region.
iii. *C:* Thermomechanically affected zone (TMAZ): The microstructure and the mechanical properties have been changed and in contrast to the HAZ zone, the FSW tool has plastically deformed the material. Between the TMAZ zone and the recrystallized side (weld nugget), there is a distinct boundary [3].
iv. *D:* Weld nugget: The area which is called the stir zone, is a totally recrystallized region. Since the grain structure is 10 times smaller than the parent material, the mechanical properties and the fracture strength are significantly changed. The diameter of the zone is a little greater than the pin diameter, but significantly smaller than the shoulder diameter [4].

Fig. 6 represents the weld zone and region nomenclatures in a friction stir welded Al alloy, as mentioned above [3].

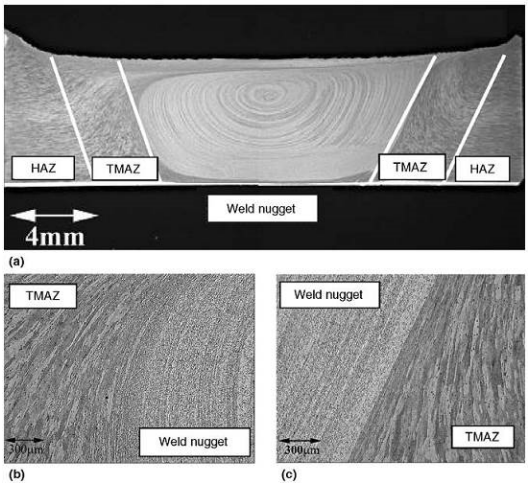

Fig. 6 (a) Micrograph viewing the weld zones and regions, (b) Retreating side, (c) Advancing side

C. Tool Type and Geometry

Tool geometry affects the traverse force, torque, and heat generation rate generated by the tool. The material flow during plasticized transformation is affected by the tool geometry as

well as the linear and rotational motion of the tool. In this respect, the shoulder diameter, shoulder surface angle, pin diameter and height are the important parameters [5].

D.Shoulder Types

1. Scroll Shoulder and Applications

Fig. 7 represents the applications of scroll shoulder and experimented welding parameters used for FSW and FSWW of several alloy materials [3]-[5].

2. Convex Shoulder and Applications

Fig. 8 represents shows the applications of scroll shoulder and experimented welding parameters used for FSW of several alloy materials [3]-[5].

Workpiece Material	Alloys	Material Thickness	Welding Parameters	Advantages	Disadvantages	Schematic View
Al	Al 5xxx (Mg alloy) series, (AA 5083 H131)	1-30 mm	250 rpm, 107 mm/min	* Because of that the channels direct deformed material from the edge of the shoulder to the pin, that way eliminating the need to tilt the tool. * Eliminates the undercut produced by the concave tool and a corresponding reduction in flash. * Due to the fact that the tool is normal to the workpiece, comparing to the concave shoulder, the normal forces are lower than needed	* It's not able to be given enough form in the different material thicknesses.	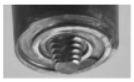
	Al 6xxx (Si ve Mg alloys) series (AA 6111-T4 - FSSW: friction stir spot welding , AA 6082-T6)		* AA 6111-T4 - 2000 rpm, dwell time; 2.5 s, plunge rate ; 2.5 mm/s. * AA 6082-T6 - 1810 rpm, 460 mm/min			
	Al 7xxx (Zn alloy) series (AA 7075-T7351)		394 and 457 rpm, 300-540 mm/min			

Fig. 7 Scroll shoulder and experimented applications

Workpiece Material	Alloys	Material Thickness	Welding Parameters	Advantages	Disadvantages	Schematic View
Al	Al 5xxx (Mg alloy) series (AA 5754 - FSSW: friction stir spot welding)	1.32 mm	1500 rpm, dwell time; 2 s, plunge rate ; 20 mm/s.	* The outer edge of the tool does not need to be contacted with the workpiece, that way the shoulder can be engaged with the workpiece at any location along the convex surface. Additionally, this shape improves the joint mismatch tolerance, enables to weld different thick materials and improves the ability to weld complex curvatures. * This shoulder minimizes the flash and welding mistakes	* The only reported succes with a thin 0.4 mm material was welded by TWI. * For the thicker material, the convex shoulder tool has also scroll shape.	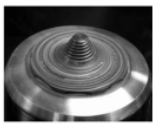
Ti	Ti-15V-3Cr-3Al-3Sr	3 mm	400 rpm, 60 mm/min, under Ar shield			
Stainless Steel	Super austenitic steels (NSSC 270)	6 mm	400-800 rpm, 76 mm /min, under Ar shield			

Fig. 8 Convex shoulder and experimented applications

3. Concave Shoulder and Applications

Fig. 9 represents the applications of concave shoulder and experimented welding parameters used for FSW and FSWW of several alloy materials [3]-[5].

E. Pin Types

1. Cylindrical Pin and Applications

Fig. 10 represents the applications of cylindrical pin and experimented welding parameters used for FSW and FSWW of several alloy materials [3]-[5].

2. Tapered Pin and Applications

Fig. 11 represents the applications of tapered pin and experimented welding parameters used for FSW and FSWW of several alloy materials [3]-[5].

3. Whorl Pin and Applications

Fig. 12 represents the applications of whorl pin and experimented welding parameters used for FSW of several alloy materials [3]-[5].

Workpiece Material	Alloys	Material Thickness	Welding Parameters	Advantages	Disadvantages	Schematic View
Al	Al 5xxx (Mg alloy) series (AA 5754 - FSSW: friction stir spot welding)	1.32 mm	1500 rpm, dwell time; 2 s, plunge rate ; 20 mm/s	* This shoulder produces quality welding and decreases significantly welding mistakes in tne microstructure and geometry * It improves the max plunge force and plunge deepth. * Simply designed.	* It produces moderate the flush and welding mistakes.	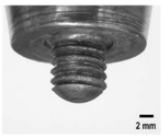
	Al 6xxx (Si ve Mg alloys) series (AA 6061-T6)	6.3 mm	286-1150 rpm, 30-210 mm/min			
	Al 7xxx (Zn alloy) series (AA 7020-T6)	4 mm	300-1620 rpm, 100-900 mm/min			
Ti	AA 1050 with 22MnB5 steel	3 mm	1000-2000 rpm, dwell time; 2 s, FSSW lap			
	Ti alloy (cp-Ti, commercially pure Ti)	1.8 mm	200 rpm, 50 mm/min, under Ar shield			
	2024-T3 Al with Ti–6Al–4V alloy	2 mm	800 rpm, 80 mm/min			
Stainless Steel	SAF 2507 super duplex	4 mm	450 rpm, 60 mm/min	* Proper operation of this shoulder design requires tilting the tool 2 to 4° from the normal of the workpiece away from the direction of travel; this is necessary to maintain the material reservoir and to enable the trailing edge of the shoulder tool to produce a compressive forging force on the weld.		
	15-5PH (martensitic, precipitation-hardening material with chromium, nickel and copper)	2.6 mm	300-450 rpm, 60-350 mm/min			
Advanced High-Strength Steels (AHSS)	DP 780 carbon steel (Dual phase, for the automotive industry, consists of a soft ferrite phase with dispersed islands of a hard martensitic phase) - FSSW	1.5 mm	800-1600 rpm, dwell time; 1-10 s			
	DP 590 carbon steel (Dual phase, for the automotive industry, consists of a soft ferrite phase with dispersed islands of a hard martensitic phase)	1.2 mm	3000 rpm, under Ar shield, FSSW lap welding			

Fig. 9 Concave shoulder and experimented applications

4. MX Triflute Pin and Applications

Fig. 13 represents the applications of MX Triflute pin and experimented welding parameters used for FSW of several alloy materials [3]-[5].

5. MX Trivex Pin and Applications

Fig. 14 represents the applications of MX Trivex pin and experimented welding parameters used for FSW of several alloy materials [3]-[5].

6. Threadless Pin and Applications

Fig. 15 represents the applications of threadless pin and experimented welding parameters used for FSW of several alloy materials [3]-[5].

III. Kevlar Material Properties and Applications

Kevlar® is a class strong and synthetic fiber which has a unique combination of characteristics such as high strength, toughness and thermal stability, is characterized from other commercial fibers [6].

Kevlar® is a registered trademark of E. I. Du Pont de Nemours and in the aromatic polyamide (aramids) family. It was developed for aerospace, defense and military industries for demanding applications [6].

There are two types of Kevlar®, Kevlar® 29 and Kevlar® 49 and especially Kevlar® 49 is widely used in aerospace industry [7]. Major applications of Kevlar® are cut, heat, and bullet-fragment resistant apparel, brake and transmission friction parts, gaskets, ropes and cables, composites, fiber-optic cables, circuit-board reinforcement, sporting goods, tires, automotive belts and hoses.

Continuous filament yarn, staple, wet and dry pulp floc, cord are the major forms of Kevlar® [7]. When we look to the properties of special interests of Kevlar®, we can see that how

Kevlar® is important for many industries [7]:

i. High tensile strength at low weight.
ii. Low elongation to break.
iii. High modulus (structural rigidity).
iv. Low electrical conductivity.
v. High chemical resistance.
vi. Low thermal shrinkage.
vii. High toughness (work-to-break).
viii. Excellent dimensional stability.
ix. High cut resistance.
x. Flame resistant.
xi. Self-extinguishing.

Table I illustrates the mechanical properties of fiber materials including Kevlar® 29 and Kevlar®49 [8].

TABLE I
THE MECHANICAL PROPERTIES OF THE FIBER MATERIALS

Material	Density (kg/m³)	Elasticity Module (MPa x 10³)	Tensile Strength (MPa)
E-glass	2550	71.7	1780
S-glass	2490	85.4	3240
Boron	2600	400	3270
High strength graphite	1780	275	2750
High module graphite	1920	515	2400
Middle class graphite	1750	220	2070
Kevlar® 29	1470	131	2750
Kevlar® 49	1470	82.5	2950

Workpiece Material	Alloys	Material Thickness	Welding Parameters	Advantages	Disadvantages	Schematic View
Mg	AZ31 Mg (Al with Mg alloy , for the aviation industry)	1.5 mm	SD: 10 mm, PD: 4 mm, PL: 1.8 mm; PS: straight circular threaded, 3 flats with M4 threads. 1000-3000 rpm, dwell time; 1.4 s, plunge rate ; 0-10 mm/s, FSSW: friction stir spot welding			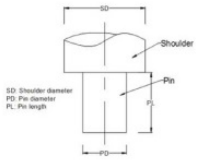
	AZ31B-H24 (Mg alloy, tempered, for the aviaton industry and electronic device cases)	2 mm	PD: 3.175 mm. PL: 1.65 mm; PS: straight circular. left (right) handed thread. 1000-2000 rpm. 300-1800 mm/min			
Al	Al alloys	5 mm	SD: 15 mm. PL: 4.7 / 6 mm; PS: concave. triangular circular threaded. 600-1500 rpm. 25-1000 mm/min	* By means of the threads, it enables to transport material from the shoulder to the pin bottom. * By means of rounded thread end to the pin tool, it reduces the tool wear and improves the welding quality. The proper dome radius was specified as 75% of the pin diameter. * Simplify produced * Welding mistakes poteintial is reduced by this design.	* A larger round-bottom pin radius will reduce the velocity differential. * The flat bottom pins need much more plunge force than others. * Max 12 mm material thickness was welded.	
	6082-T6 Al	1.5 mm	PD: 1.7 mm; PS: concave; PL: 1.2mm. 1810 rpm. 460 mm/min			
	6061-T6 Al	6.3 mm	SD:26 mm; PD: 5.6 mm; PL: 5.9 mm; PS: straight circular threaded. 286–1150 rpm. 30–210 mm/min			
	7020-T6 Al	4 mm	SD: 13 mm; PS: straight circular; PL:3.19 mm: PD: 5 mm. 300–1620 rpm. 100–900 mm/min			
	51-T6 Al + 20% Al2	5 & 6 mm	SD: 19 mm; PS: straight circular threaded; PD: 6.3mm. 500–2000 rpm. 60–540 mm/min			
	09 + 20% SiC (for ca	4 mm	SD: 19 mm; PS: straight circular threaded; PD: 6. 3 mm; PL: 3.6mm. 500–1000 rpm. 360 ve 660 mm/min			
Composite	Al–10 wt-% TiB2 (wt %10 Al, Al with TiB2 alloy)	6 mm	SD: 16 mm; PS: square circular. 2000 rpm, 30 mm/min			
Ti		3 mm	'SD: 18 mm; PS: straight circular ; PD: 5 mm PL: 2.85 mm. 1250 rpm. 32 mm/s. 1500 rpm. 60 mm/min			

* SD: shoulder diameter, PL: pin length, PD: pin diameter, PS: pin shape

Fig. 10 Cylindrical pin and experimented applications

Workpiece Material	Alloys	Material Thickness	Welding Parameters	Advantages	Disadvantages	Schematic View
Al	7020-T6 Al	4 mm	SD: 13 mm; PS: straight circular, tapered circular with three flats ; PL:3.19 mm: PD: 5 mm. 300–1620 rpm, 100–900 mm/min			
	AA 1050 - 22MnB5 (Al alloy and hot stamped boron steel)	1.8 mm	SD: 12 mm; PS: Concave shoulder; PDt: 2 mm; PL: 2.7mm. FSSW (friction stir spot welding) lap joint welding; 1000–2000 rpm, dwell time: 2 s			
	AA 6061– (3–7) % TiC (Al 6061, abrasion and wear resistance and improved damping capabilities with TiC)	6 mm	PS: square, hexagonal, tapered hexagonal, tapered octagonal. 30–135 mm / min			
	2024-T3 Al with Ti–6Al–4V alloy	2 mm	SD: 18 mm; PS: threaded and tapered; PD: 6 mm. 800 rpm, 80 mm/min			
Mg	AZ31B (Mg alloy)	6 mm	SD: 15,18,21 mm, PD: 6 mm, PL: 5.7 mm; PS:triangular and square, straight circular threaded, tapered circular. 1600 rpm, 40 mm/min	* This design allows to weld the material over 12 mm thick * This pin has lower transverse loads comparing to a cylindrical pin.		
Ti	cp-Ti (commercially pure Ti)	3 mm	SD: 15 mm; PS: tapered at 45deg and truncated ; PL: 1.7 mm; PDb: 5.1mm. 200 rpm, 50 mm/min, under Ar shield	* The increased surface velocity at the bottom of the pin would increase the throwing power of the pin, or the ability of the pin to affect metal below the end of the pin. * The stepped spiral tools enable to weld high temperature resisting steel (i.e. Ni-Al bronze, survived the 1000°C temperature)	* High temperature and hydrostatic pressure can increase the tool wear.	
	Ti–6Al–4V	3-12 mm	SD: 19–32 mm; PS: tapered; PL: 2.8–13.3mm. 150–750 rpm, 50–200 mm/mm			
	Ti-5111 plate	12.7 mm	PL: 12.7 mm; PD: 25.4 mm; PDt:9.5mm. 140 rpm, 51 mm/min			
	Ti–15V–3Cr–3Al–3Sn	3 mm	SD: 15 mm; PDb: 5.1 mm; PDt: 3mm. 400 rpm, 60 mm/min, under Ar shield			
Boron	Hot stamped boron steels	1.4 mm	SD: 10.2 mm; PL: 2.3 mm; PS: tapered circular with three flats. 800–2000 rpm, 1.9–10.5 s welding time. Lap welding			
Advanced High-Strength Steels (AHSS)	DP 600 carbon steel (Dual phase, for the automotive industry, consists of a soft ferrite phase with dispersed islands of a hard martensitic phase)	1.22 mm	SD: 10 mm; PS: straight circular; PL: 1.7 mm; PD: 4–5.1mm. Plunge rate; 3000 rpm, 30–60 mm / min (FSSW)			
Composite	AA2124 / SiCp / 25-T4	3 mm	SD: 20 mm; 'PL: 25 mm; PS: tapered threaded, PDb: 6 mm; PDt: 4mm. 900 rpm, 100 mm/min			
	Al–15 wt - % Mg2Si (wt %15 Al , Al with Mg2Si alloy)	6 mm	SD: 18 mm; PS: tapered circular threaded; PL: 5.7mm. 710–1400 rpm, 125 mm / min			

* SD: shoulder diameter, PL: pin length, PD: pin diameter, PS: pin shape, PDt: pin diameter at the top (larger diameter) for tapered pin, PDb: pin diameter at the bottom (smaller diameter) for tapered pin

Fig. 11 Tapered pin and experimented applications

Workpiece Material	Alloys	Material Thickness	Welding Parameters	Advantages	Disadvantages	Schematic View
Al	6082 T6 Al	1-50 mm	Single pass	'* This design reduces the displaced volume of a cylindrical pin of the same diameter by 60%. It also decreases the traverse loads, which enables faster tool travel speeds * The difference from the truncated cone pins is to has the helical ridge on the pin surface * The significant advantages of this pin is the ratio of the volume swept by the pin to the pin volume. This ration is 1.1:1 for a cylindrical pin, while for whorl pin is 1.8:1.		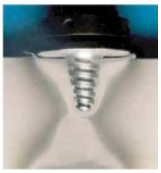
	6082 T6 Al	75 mm	Both sides, single pass			

Fig. 12 Whorl pin and experimented applications

Workpiece Material	Alloys	Material Thickness	Welding Parameters	Advantages	Disadvantages	Schematic View
Al	7075-T7351 Al	6.35 mm	394 ve 457 rpm, 300-540 mm/min	* This pin is a further refinement of the Whorl pin by TWI. Its three flutes reduce the displaced volume of a cylindrical pin by 70% and supply additional deformation at the weld line. * This designed pin has a pin volume swept to pin volume ratio of 2.6:1 (for 25 mm thick plate). * Experimental research of cast A356 Al to demonstrate that a modified Triflute pin (cylindrical pin with three flutes) is more effective in breaking up silicon particles and healing casting porosity than either cylindrical or truncated cone pins.		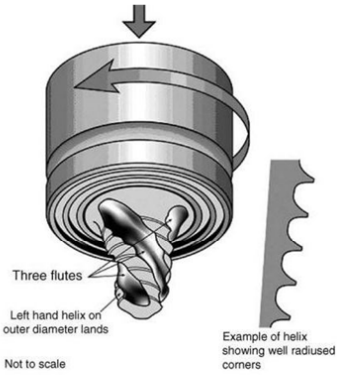
	6082 T6 Al	1-50 mm	Single pass			

Fig. 13 MX Triflute pin and experimented applications

Workpiece Material	Alloys	Material Thickness	Welding Parameters	Advantages	Disadvantages	Schematic View
Al	7075-T7351 A	6.35 mm	394 ve 457 rpm, 300-540 mm/min	* Experimental research of 6.35 mm thick 7075-T7351 Al demonstrated that the Trivex and MX-Trivex pin produced an 18 to 25% reduction of traversing forces and a 12% reduction in forging forces in comparison to an MX Triflute pin. * The materials that were welded with this pin, had a considerable increased in tensile strength.		

Fig. 14 MX Trivex pin and experimented applications

Workpiece Material	Alloys	Material Thickness	Welding Parameters	Advantages	Disadvantages	Schematic View
Al	7075-T7351 Al	2.4 mm		* This pin is applicable for welding applications of high temperature or highly abrasive composite alloys under aggressive environment. Especially, with PCBN (Polycrystalline cubic boron nitride, is extremely hard and thermally stable, and provides extreme resistance to deformation and wear at high temperatures) or tungsten carbide (WC) coated pins are able to achieve better welding results. * Welding with a thin sheet, such as 0.4 mm can be obtained good results.		
	2024-T3 Al	2.11 mm				
Mg	Mg AZ31 (Al with Mg alloy, for the aviation industry)	0.4 mm				
Ti	21S Ti (high-strength, oxidation resistant strip alloy, for aerospace industry)	1.2 mm				

Fig. 15 Threadless pin and experimented applications

In this study, as seen in Fig. 16, Twaron CT 736 PHF Kevlar® resin material was used which is a registered trademark of SAATI S.p.A. [7].

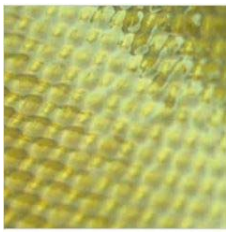

Fig. 16 The resinous fiber view of Twaron CT 736 PHF

Table II illustrates the mechanical properties of Twaron CT 736 PHF compared to Kevlar® 29 and Kevlar®49 [6], [7]. It can be seen that they have similar mechanical properties.

TABLE II
THE MECHANICAL PROPERTIES OF THE FIBER MATERIALS

Properties	Unit	Twaron CT 736	Kevlar 29	Kevlar 49
Density	g/cm^3	1.44	1.44	1.44
Tensile Strength	GPa	2.4-3.6	3.6	3.6
Tenacity	N/tex	1.65-2.5	2.03	2.08
Tensile Module	GPa	60-120	70.5	112.4
Elongation	%	2.2-4.4	3.6	2.4
Moisture	wt%	3.2-5	4.5	3.5
Decomposition or Melting	ºC	500	427-482	427-482
Specific Heat				
At 25°C	cal/gºC	0.34	0.34	0.34
At 100°C	cal/gºC	0.48	0.48	0.48
At 180°C	cal/gºC	0.6	0.6	0.6
Thermal Conductivity	W/mK	0.04	0.04	0.04

Table III makes a comparison between the mechanical properties comparing of some other material with Kevlar®.

TABLE III
SOME OTHER MATERIALS COMPARED TO KEVLAR

Material	Strength to weight KN.m/kg.	Ultimate Strength MPa	Density g/cm^3
Kevlar® (ARAMID)	2514	2757	1.44
Steel alloy ASTM A36	254	400	7.8
Aluminium alloy	222	248-483	2.63 - 2.8
Spider Silk	1069	1000	1.3
Oak	87	65	0.75

IV. Model Analysis of Heat Generation in FSW

In recent years, analytical models based on a cylindrical pin structure were developed [9]. Since the tapered pin has better mechanical properties than straight the cylindrical pin, in this study, as seen in Fig. 17, a tapered circular pin with 3 flat layers was used and the analytical model was developed accordingly.

Fig. 17 A tapered circular with 3 flats pin used in this study

A. Estimation of the Heat Generation Model

As shown in Fig. 18, heat generation occurs at three different regions where Q_1 is under the tool shoulder, Q_2 is at the pin side surface and Q_3 is at the pin tip. The total heat generation is obtained via $Q_{total} = Q_1 + Q_2 + Q_3$ [9].

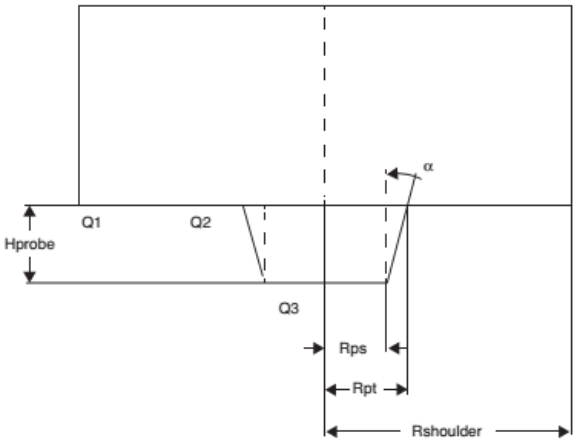

Fig. 18 Schematic view of heat generation regions at a tapered pin

In Fig. 19, the nomenclature is listed that is used during estimation [9]. For the analytical model, the following assumptions were made and accepted [9]:

i. The estimation based upon uniform contact shear stress ($\tau_{contact}$) was considered.
ii. The shearing takes place at the contact interface during sliding.
iii. Deformation mechanism was not considered.
iv. Since friction interface mechanism, the friction shear stress $\tau_{friction}$ was considered. For the sliding condition, the friction shear stress was estimated via $\tau_{contact} = \tau_{friction} = \mu p = \mu\sigma$.

Q_1	heat generation from shoulder surface
Q_2	heat generation from pin surface
Q_3	heat generation from pin tip surface
μ	friction coefficient
ω	tool angular rotation speed (rpm)
α	pin taper angular (°)
ϑ	tool speed (mm/min)
σ	contact pressure (Pa)
$\tau_{contact}$	contact shear stress (Pa)
R_{PT}	pin tip radius (mm)
R_{PS}	pin bottom radius (mm)
$R_{shoulder}$	tool shoulder radius (mm)
Q_{total}	total heat generation (W)
H_{probe}	pin length (mm)

Fig. 19 Nomenclature

A tool with flat shoulder, taper circular pin and flat probe tip is accepted which is a modified version of the one given by [9]. The tapered pin surface is indicated by the taper angle α. The general heat generation equation is:

$$dQ = \omega.dM = \omega.r.dF = \omega.r.\tau_{contact}.dA \qquad (1)$$

Fig. 20 illustrates the contact surface between tool and workpiece given by position and orientation with regard to rotation axis [9].

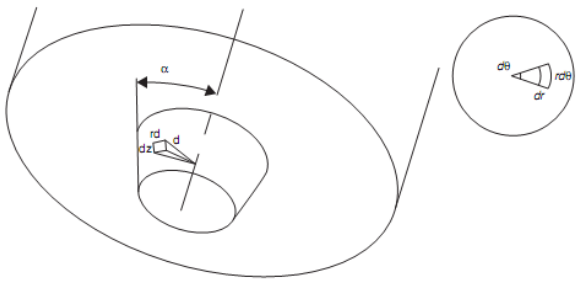

Fig. 20 For a tapered pin, surface position and infinitesimal segments

1. Heat Generation of the Tool Shoulder Surface

To estimate the heat generation of the tool shoulder surface around the tool center axis, an infinitesimal area is approached [9]. $dA = r.d\theta.dr$ is the infinitesimal area that is exposed to the uniform contact shear stress $\tau_{contact}$ [9]. The mentioned

area provides an infinitesimal force of $dF = \tau_{contact}.dA$ and torque of $dM = r.dF$. Thereby, the heat generation of the area is achieved;

$$dQ = \omega.r.dF = \omega.r^2.\tau_{contact}.d\theta.dr \quad (2)$$

where ω is the angular velocity, r is the distance to the center of rotation, $r.d\theta$ and dr are the segment dimensions [9]. Integrating (2), the heat generation is achieved from R_{PT} to $R_{shoulder}$ and thereby, it gives that [9]:

$$Q_1 = \int_0^{2\pi}\int_{R_{PT}}^{R_{shoulder}} \omega.r^2.\tau_{contact}.d\theta.dr$$
$$Q_1 = \frac{2}{3}\pi.\omega.\tau_{contact}.(R_{shoulder}^3 - R_{PT}^3) \quad (3)$$

2. Heat Generation of the Tapered Pin Surface

Equation (4) expresses the heat generation of the tapered pin surface over the probe side area [9]:

$$Q_2 = \int_0^{2\pi}\int_0^{l} \omega.r^2.\tau_{contact}.d\theta.dz$$
$$Q_2 = 2.\pi.\omega.\tau_{contact}.l.\left(\frac{R_{PS}+R_{PT}}{2}\right)^2$$
$$Q_2 = \frac{\pi.\omega.\tau_{contact}}{2}.\frac{H_{probe}}{cos\alpha}.(R_{PS}+R_{PT})^2 \quad (4)$$

3. Heat Generation of the Pin Tip Surface

Integrating (1) and assuming a flat pin tip, it gives (5) as follows [9]:

$$Q_3 = \int_0^{2\pi}\int_0^{R_{PS}} \omega.r^2.\tau_{contact}.d\theta.dz$$
$$Q_3 = \frac{2}{3}\pi.\omega.\tau_{contact}.R_{PS}^3 \quad (5)$$

Now, Q_{total} can be calculated with using (3)–(5) as follows:

$$Q_{total} = Q_1 + Q_2 + Q_3$$

$$Q_{total} = \frac{2}{3}\pi.\omega.\tau_{contact}.(R_{shoulder}^3 - R_{PT}^3) + \frac{\pi.\omega.\tau_{contact}}{2}.\frac{H_{probe}}{cos\alpha}.(R_{PS}+R_{PT})^2 + \frac{2}{3}\pi.\omega.\tau_{contact}.R_{PS}^3$$

However, since $R_{PS} = R_{PT} - H_{probe}.tan\alpha$, Q_{total} becomes;

$$Q_{total} = \frac{2}{3}\pi.\omega.\tau_{contact}.\left(R_{shoulder}^3 - R_{PT}^3 + \frac{3}{4}.\frac{H_{probe}}{cos\alpha}.(2.R_{PT} - H_{probe}.tan\alpha)^2 + (R_{PT} - H_{probe}.tan\alpha)^3\right) \quad (6)$$

If requested, the energy input per unit length of the weld can be achieved by dividing (6) by the transverse velocity as [9]:

$$Q_{energy/length} = \frac{2}{3}.\frac{\omega.F.\mu}{\vartheta.R_{shoulder}^2}.\left(R_{shoulder}^3 - R_{PT}^3 + \frac{3}{4}.\frac{H_{probe}}{cos\alpha}.(2.R_{PT} - H_{probe}.tan\alpha)^2 + (R_{PT} - H_{probe}.tan\alpha)^3\right) \quad (7)$$

For a cylindrical pin, since $R_{PS} = R_{PT}$, Q_{total} becomes simplified as follow [9];

$$Q_{total} = \frac{2}{3}.\pi.\omega.\tau_{contact}.\left(R_{shoulder}^3 + 3.H_{probe}.R_{PS}^2\right) \quad (8)$$

B. Numerical Approach

1. Estimation of the Heat Transfer

When estimating heat transfer in the plate, (9) was based on finite element analysis:

$$\rho C_p\frac{\partial T}{\partial t} + \rho C_p u\cdot\nabla T = \nabla\cdot(k\nabla T) + Q \quad (9)$$

where T is heat, t is time, u is unit vector; ρ, k and Cp are material parameters which represents respectively density, thermal conductivity and specific heat capacity. When fixing the coordinate system to the welding tool, (9) becomes (10) includes a convective term in addition to the conductive term, as follows [10]:

$$\nabla\cdot(-k\nabla T) = Q - \rho C_p u\cdot\nabla T \quad (10)$$

The following definition explains the boundary conditions in order to obtain heat generation between the plates, pin and the shoulder [10];

$$Q(r,T) = \begin{cases} \left(\frac{\mu F_n}{A_s}\right)\omega r; T < T_{melt} \\ 0; T \geq T_{melt} \end{cases} \quad (11)$$

where F_n is the nominal force, A_s is the shoulder surface area, T_{melt} is Kevlar®'s melting temperature, μ is Kevlar®'s friction coefficient, ω is the angular velocity, r is the pin radius.

2. Estimation of the Torque

The required torque input for the fully stick condition was estimated following the discussion by [11]. Reynolds divided the total torque into three parts as follows [12]:

$$M = M_{shoulder} + M_{pin\ surface} + M_{pin\ bottom}$$
$$\Rightarrow M = \frac{\int_{r_i}^{r_0} r\tau 2\pi r dr}{2} + \int_0^{r_i} r\tau 2\pi r dr + r_i\tau 2\pi r_i h \quad (12)$$

where r_i is the pin radius, r_0 is the shoulder radius, τ is the shear stress and h is the pin length. When we take $\tau = \sigma/\sqrt{3}$ where σ presents the shear strength, the equation becomes [12]:

$$M = \frac{2\pi\sigma}{\sqrt{3}}\left[\frac{\int_{R_{PS}}^{R_{shoulder}} r^2 dr}{2} + \int_0^{R_{PS}} r^2 dr + {R_{PS}}^2 H_{probe}\right] \quad (13)$$

Equation (13) was obtained in accordance with a straight pin approach, but if the tapered part of the pin extends to the pin tip, then we can acquire 90% of the torque from (13) [13]. For this reason, we used this equation in order to estimate the torque.

Fig. 21 illustrates the dimensions of the pin used in our study where R_{PS} is the pin bottom radius, R_{PT} is the pin tip radius, H_{probe} is the pin length and $R_{shoulder}$ is the shoulder radius;

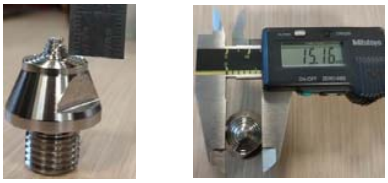

(a) (b)

(c) (d)

Fig. 21 The dimension of the pin used in our study: a) The pin length ($H_{probe} = 35\ mm$), b) The shoulder diameter ($R_{shoulder} = 7.5\ mm$), c) The pin bottom diameter ($R_{PS} = 3\ mm$, the diameter is accepted 6 mm), d) The pin tip diameter ($R_{PT} = 1.6\ mm$)

$$\sigma = 3600x10^3\ Pa,\ R_{PS} = 0.003\ m,$$
$$R_{shoulder} = 0.0075\ m,\ H_{probe} = 0.0035\ m$$

was taken and the torque was estimated as follows:

$$M = \frac{2\pi\sigma}{\sqrt{3}}\left[\frac{\int_{R_{PS}}^{R_{shoulder}} r^2 dr}{2} + \int_0^{R_{PS}} r^2 dr + {R_{PS}}^2 H_{probe}\right] = 5.7\ Nm$$

3. Estimation of the Plunge Force

In order to produce a Kevlar® plate from some Kevlar® fabrics, as seen in Fig. 22, the fabrics were pressed at 165°C temperature and 6 bar in 10 minutes. Fig. 23 illustrates the produced plates which have 150 mm x 250 mm x 4 mm dimensions.

Fig. 22 The process of producing Kevlar® plates

Fig. 23 The dimensions of Kevlar® plate produced for this study

The required plunge force during pressing Kevlar® fabrics is also used as a reference in order to estimate the plunge force for the plates. As seen below calculation, P is the applied pressure, A_p is the plate surface area, and F is the applied plunge force and it was calculated as follows:

$$P = 6\ bar = 6x10^5\ Pa, A_p = 0.15x0.25\ m^2$$
$$P = \frac{F}{A_p} \Rightarrow 6x10^5 = \frac{F}{0.15x0.25} \Rightarrow F = 2250\ N$$

According to a literature research, the plunge force is declared as a force which is applied to the workpiece by the milling machine and expressed as in (14) as follows [14]:

$$F \cong 6\pi\ {R_{shoulder}}^2 \tau \quad (14)$$

Calculating the plunge force according to this equation we obtain:

$$F = 6\pi(0.0075)^2 \frac{3600x10^3}{\sqrt{3}} = 2203\ N$$

It can be seen that this value is approximately closed to the required plunge force value during pressing of Kevlar® fabrics (2250 N).

4. Estimation of Friction Coefficient

As reported by an experimental research, the friction coefficient (μ) of Kevlar® for the static condition is calculated between 0.36-0.51 [15]. In this study, it was estimated theoretically as follows:

$$\mu = \frac{M}{Fx\ R_{shoulder}} = \frac{5.7}{2203x0.0075} = 0.34$$

which is close to the experimental values ranging from 0.36 to 0.51thus, $\mu = 0.35$ was accepted.

5. Estimation of Non-Newtonian Fluid

In a non-Newtonian fluid, the ratio between the local shear stress and the local shear rate cannot be calculated via Newton's laws. In this condition, the fluid is not a fixed scaler, but a variable and viscosity can change when under force to either more liquid or more solid. For instance; ketchup, cream, toothpaste, blood and shampoo are non-Newtonian fluids.

In this study, Carreau model we also used Carreau model was assumed in CFD analysis. The main reason for nonlinear viscosity is the existence of high and low strain rates together around the pin and the boundary of the TMAZ [16]. Fig. 24 shows the classification of non-Newtonian fluids [17].

Based on the flow behavior index, *n* [17]:

i. If 0 < n < 1; the fluid shows pseudoplastic or shear thinning behavior. A smaller *n* value means a greater degree of shear thinning.
ii. If *n* = 1; Newtonian behavior.
iii. If 1 < *n*; the fluid shows dilatant or shear thickening. Comparing to pseudoplastic behavior, an increase in the fluid viscosity with an increase in the shear rate. A greater *n* means a greater degree of shear thickening.

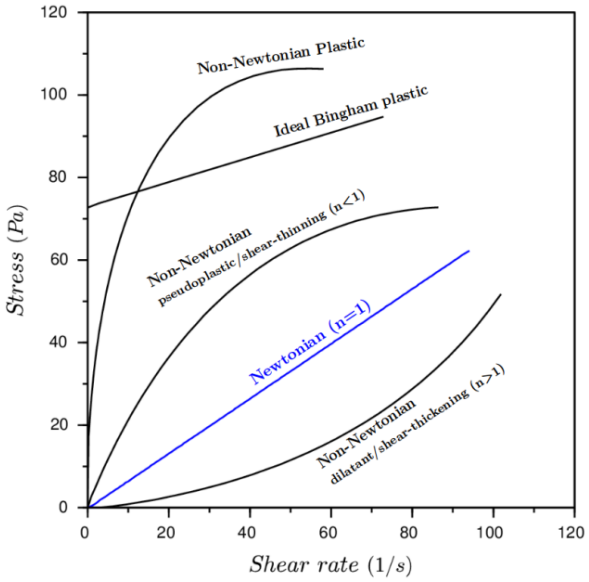

Fig. 24 The general types of non-Newtonian fluids and their stress-strain behavior

Carreau model is defined by;

$$\mu = \mu_\infty + (\mu_0 - \mu_\infty)\left[1 + \left(\dot{\gamma}\lambda \exp\left(\frac{T_0}{T}\right)\right)^2\right]^{\frac{(n-1)}{2}} \quad (15)$$

where μ_∞ is the infinite shear viscosity (kg/ms), μ_0 is the zero shear viscosity (kg/ms), $\dot{\gamma}$ is the shear strain rate $(1/s)$, λ is the time constant, T is the melting temperature (K), T_0 is the reference temperature (K), n is the power law non-Newtonian fluid index.

In this study, the constants were found to be [18]-[20].

$$\mu_0 = 10^4\ kg/ms,\ \mu_\infty = 0,\ \dot{\gamma} = 0.1\ 1/s\ ,\ \lambda = 10\ ,\ T = 441\ K\ (168\ °C),\ T_0 = 298\ K\ (25\ °C),\ n = 0.2$$

Hence, μ was calculated as:

$$\mu = \mu_\infty + (\mu_0 - \mu_\infty)\left[1 + \left(\dot{\gamma}\lambda exp\left(\frac{T_0}{T}\right)\right)^2\right]^{\frac{(n-1)}{2}} = 0 + (10^4 - 0)x\left[1 + \left(0.1x10xexp\left(\frac{298}{441}\right)\right)^2\right]^{\frac{(0.2-1)}{2}} = 5.32x10^3 \text{ kg/ms}$$

V. Analyzing Computational Fluid Dynamics (CFD) of the Model

The Finite Element Analysis (FEA) of the FSW system was performed by using COMSOL Multiphysics. CFD and Heat Transfer modules were employed together in a multiphysics setting. The geometry was defined as a 200 mm x 200 mm x 4 mm thick block in Fig. 25. Tip of the pin was defined as a taper shape and back of it was defined as a pillbox, as seen in Fig. 26.

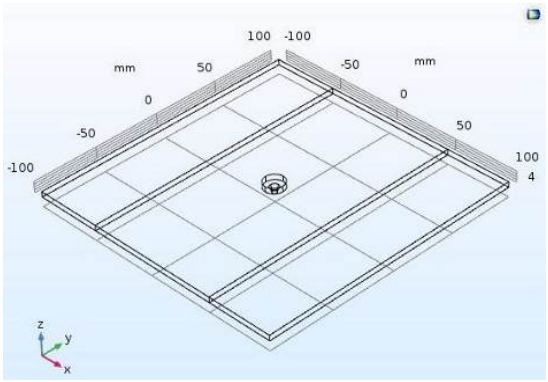

Fig. 25 Definition of the problem in COMSOL

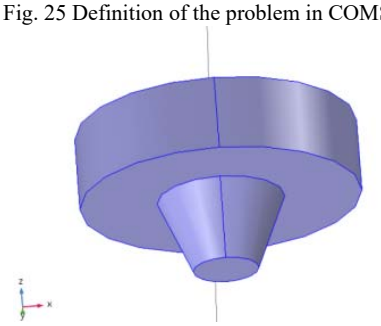

Fig. 26 FSW pin as described in COMSOL

Non-Newtonian Carreau model was adopted for the solution as seen in Fig. 27.

The displacement of the Kevlar® material was modelled as a viscous flow. In Fig. 28, rotation of the pin was modelled as a sliding wall.

Heat generated by the pin rotation was modelled as boundary sources on the shoulder and on the pin surface.

Meshing has been made via tetrahedral meshing. Mesh on all domains consisted of 156154 elements with an average quality of 0.6617, which was fair enough, as seen in Fig. 29.

Calculations were performed for two parameters: *u_weld*, the travelling velocity and *w*, the rotational velocity of the pin. Required *u_weld* and *w* values were calculated to be respectively 80 mm/min and 300 rpm in 5 seconds. Velocity maps for two different parameter set are represented in Figs. 30 and 31. Here the translational velocity is subtracted.

It is not readily seen from the two images above whether the desired mixing was achieved. In order to do that we needed a picture which shows velocity vectors. A full circular motion is expected around the pin. Any vortex like field at either side of the pin reveals absence of the desired mixing condition. Below two figures for two set of parameters one of which exhibits a clear vortex in Fig. 32 which does not appear in the other one as given in Fig. 33.

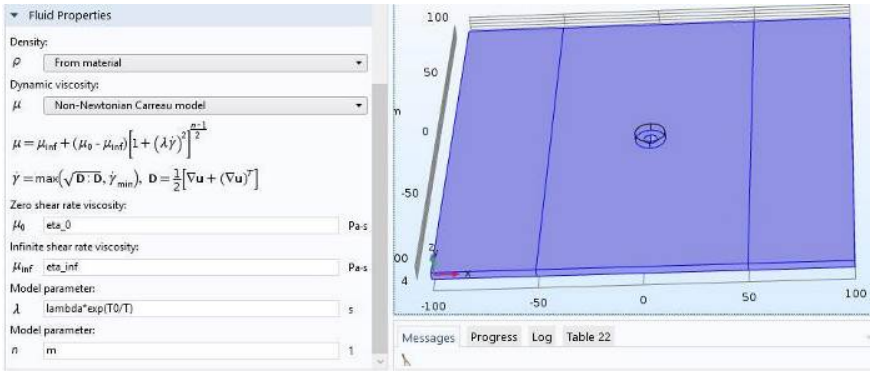

Fig. 27 Non-Newtonian Carreau model setting in COMSOL

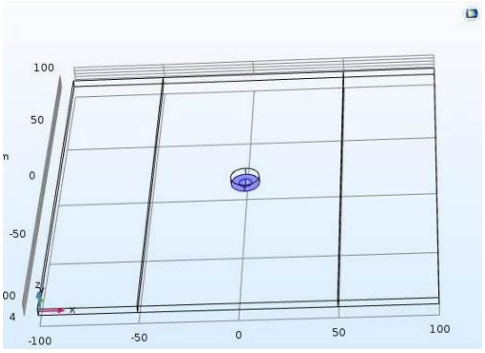

Fig. 28 Pin velocity and rotation setting in COMSOL

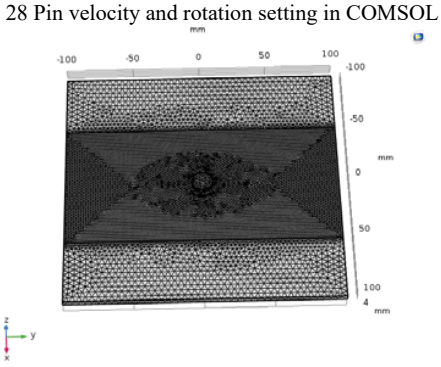

Fig. 29 Mesh structure used for the solution

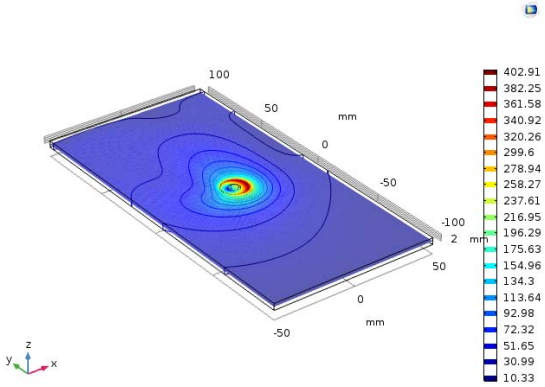

Fig. 30 Velocity map for u_weld = 100 mm/min and w = 400 rpm

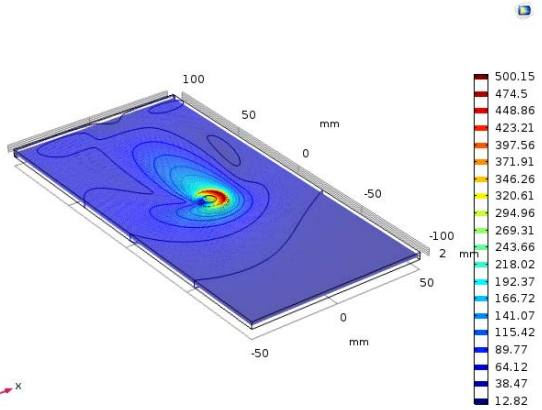

Fig. 31 Velocity map for u_weld = 200 mm/min and w = 400 rpm

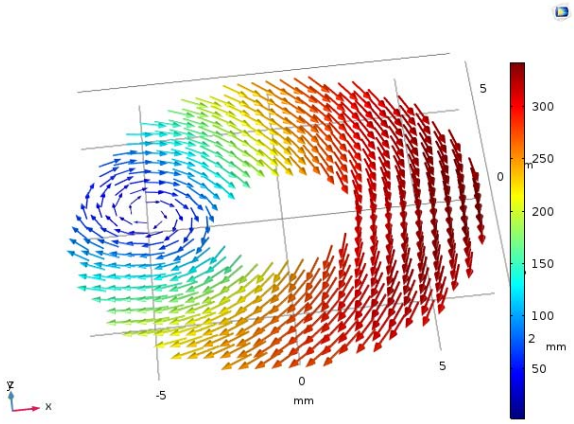

Fig. 32 Velocity vectors for u_weld = 200 mm/min and w = 400 rpm

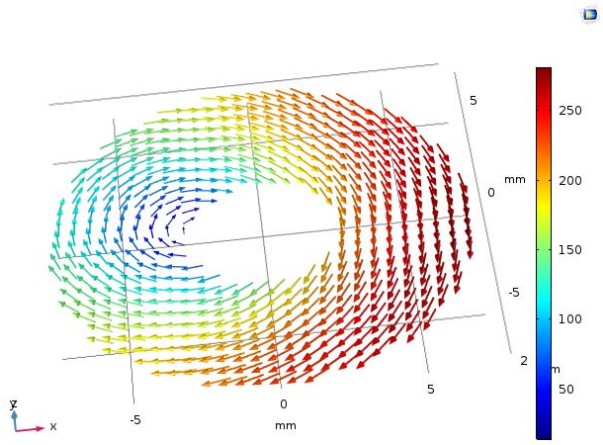

Fig. 33 Velocity vectors for u_weld = 100 mm/min and w = 400 rpm

Uniform distribution of the shear rate can be another clue for determining the mixing condition as seen in Figs. 34 and 35. Table IV shows all the parameters which were calculated. It can be seen that for welding velocities above 100 mm/min mixing does not occur. Rotation velocity must be high enough to facilitate the mixing however there is a compromise between mixing and overheating which can be elevated for increased rotational speeds.

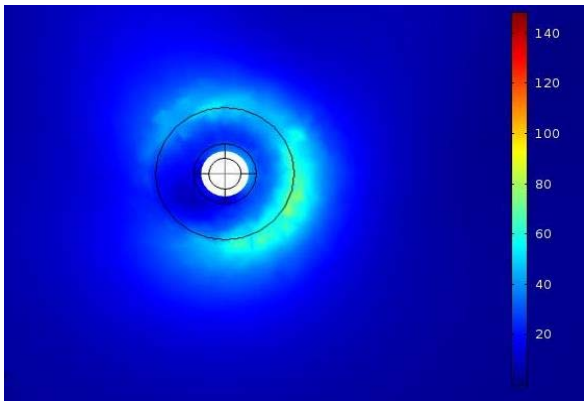

Fig. 34 Shear rate for u_weld = 200 mm/min and w = 400 rpm

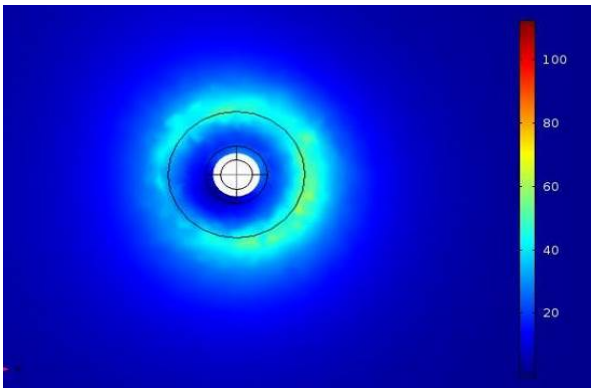

Fig. 35 Shear rate for u_weld = 100 mm/min and w = 400 rpm

TABLE IV
MIXING COMPARISON FOR DIFFERENT PARAMETERS

Welding Velocity (mm/min) \ Rotational Velocity (rpm)	50	100	150	250	300	350	400	500	600
30	×	×	✓	✓	✓	✓	✓	✓	✓
40	×	×	×	✓	✓	✓	✓	✓	✓
50	×	×	×	✓	✓	✓	✓	✓	✓
60	×	×	×	✓	✓	✓	✓	✓	✓
70	×	×	×	×	✓	✓	✓	✓	✓
80	×	×	×	×	×	✓	✓	✓	✓
90	×	×	×	×	×	✓	✓	✓	✓
100	×	×	×	×	×	×	✓	✓	✓
200	×	×	×	×	×	×	×	×	×
300	×	×	×	×	×	×	×	×	×

Thus, the translational velocity must not be too high to prevent the mixing. But on the other hand, in case the welding velocity is very low this will cause overheating of the sample and will burn it. In order to check this, temperature map of the system was also calculated. It is required not to exceed 170°C. An isothermal surface map around the pin for a certain set of parameters can be seen in Fig. 36.

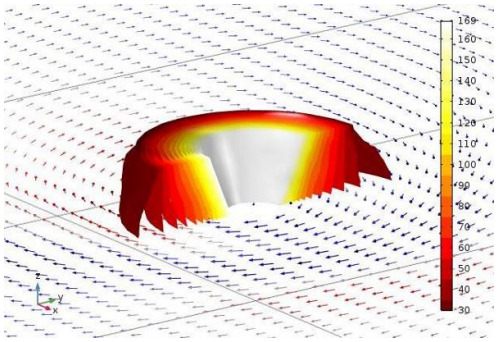

Fig. 36 An isothermal surface map around the pin. Here isothermal surfaces are shown only for negative x values for a better view

VI. EXPERIMENTAL PROCEDURES

A. Setup

In order to perform friction stir processing (FSP), Smart XL6036 horizontal knee-type milling machine was used, as seen Fig. 37.

Fig. 37 Smart XL6036 horizontal knee-type milling machine

To check the temperature and investigate the thermal situation during FSP, FLIR T450sc thermal camera was used, as seen in Fig. 38.

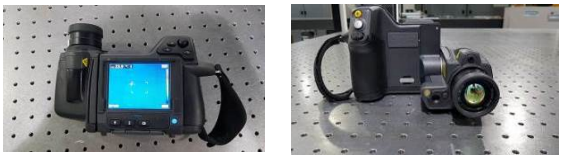

Fig. 38 FLIR T450sc thermal camera

Fig. 39 illustrates the setup of the milling machine and the name of the parts used in FSP.

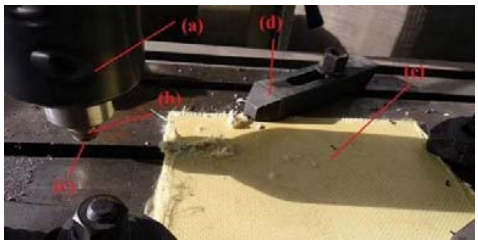

Fig. 39 The setup of the milling machine used in FSP; (a) Spindle, (b) Pin holder, (c) Pin, (d) Fixture, (e) Kevlar® plate

B. Friction Stir Processing and Results

1. Processing Without Joint

In this section, during all process, only one plate was tried to weld in order to investigate the weldability of the Kevlar® plate as seen in Fig. 39. Due to the fact that COMSOL could not create any solution over 500 N plunge force, the plunge force was ignored during analysis.

As seen in Fig. 40, welding was processed at 1800 rpm and 65 mm/min, respectively, rotation speed and welding speed.

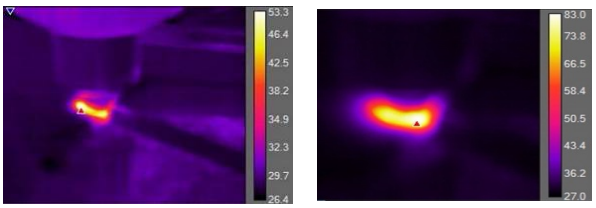

(a) (b)

Fig. 40 Processing at 1800 rpm and 65mm/min, welding was started at 53°C (a) and reached to 168°C (b) in 5 seconds

After 168°C, the temperature went up to max 328°C and then some imperfections, cluster pulp burning (like volcanic eruption) were occurred, as seen in Fig. 41.

As seen in Fig. 42 welding was processed at 720 rpm and 65 mm/min.

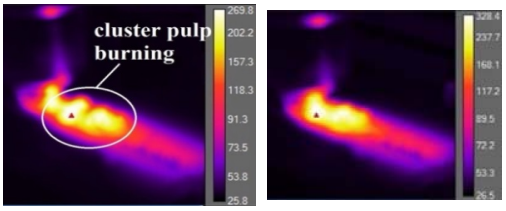

(a) (b)

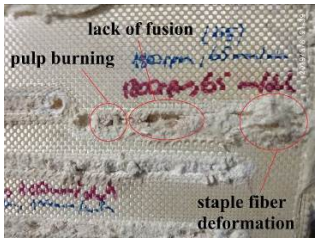

(c)

Fig. 41 Welding results at 1800 rpm and 65 mm/min; (a) Cluster pulp burning, (b) Max reached temperature, (c) Imperfections such as lack of fusion, staple fiber deformation and pulp burning

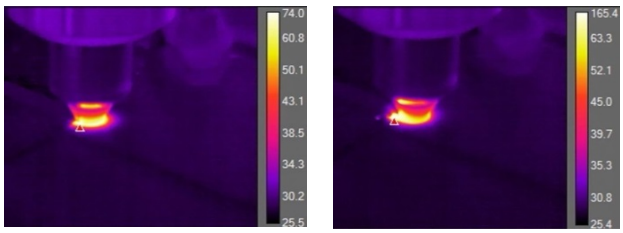

(a) (b)

Fig. 42 Processing at 720 rpm and 65 mm/min, welding was started at 74°C (a) and reached to 165°C (b) in 4 seconds

After reaching 165°C, the temperature quickly rises to 391°C and cluster pulp burning and spattering were observed (pulp burning was started at 213°C) and the temperature went up to max 481°C. Then, again some imperfections such as cluster pulp burning, spatter and lack of fusion were occurred, as seen in Fig. 43.

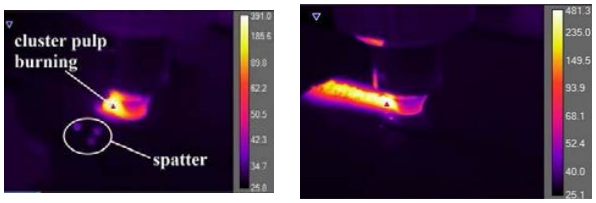

(a) (b)

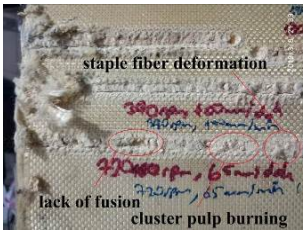

(c)

Fig. 43 Welding results at 720 rpm and 65 mm/min; (a) Cluster pulp burning and spatter, (b) Max reached temperature, (c) Imperfections such as lack of fusion, staple fiber deformation and cluster pulp burning

As seen in Fig. 44, welding was processed at 390 rpm and 100 mm/min.

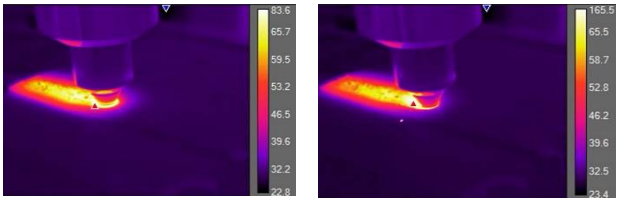

(a) (b)

Fig. 44 Processing at 390 rpm and 100 mm/min, welding was started at 83°C (a) and reached to 165°C (b) in 6 seconds

After 165°C, some pulp burning was started at 288°C and reached at max 298°C, again some imperfections like cluster pulp burning, spatter and lack of fusion were occurred, as seen in Fig. 45.

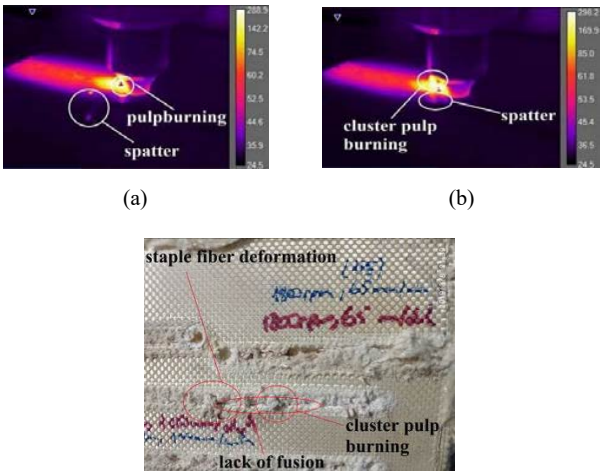

(a) (b)

(c)

Fig. 45 Welding results at 390 rpm and 100 mm/min; (a) Pulp burning and spatter, (b) Max reached temperature and again cluster pulp burning and spatter, (c) Imperfections such as lack of fusion, staple fiber deformation and cluster pulp burning

2. Processing on a Lap Joint

As seen in Fig. 46 welding was processed at 1800 rpm, 65 mm/min on a lap joint. The thickness of one plate was approximately 2 mm and totally ~4 mm. At 168°C, pulp burning was occurred, as seen in Fig. 46 (b).

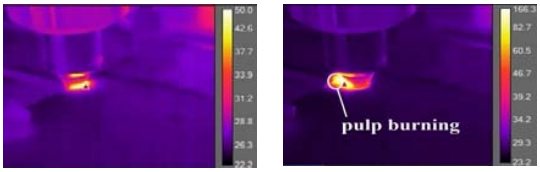

(a) (b)

Fig. 46 Processing at 1800 rpm, 65 mm/min on a lap joint, welding was started at 50°C (a) and reached to 166°C (b) in 9 seconds and pulp burning was started

After reaching at 166°C, in a short time, the temperature was escalated to max 354°C and then, more cluster pulp burning was observed as seen in Fig. 47 (a). Fig. 47 (c) illustrates that throughout the joint line, the upper plate was sheared and as seen (d), on the surface of lower part, only deformation was observed.

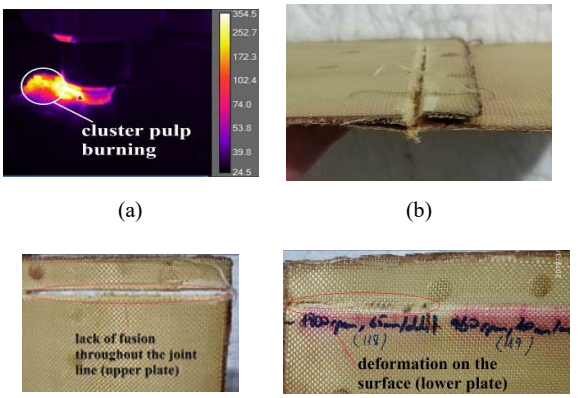

(a) (b)

(c) (d)

Fig. 47 Welding results at 1800 rpm, 65 mm/min on a lap joint; (a) At max 354°C, more cluster pulp burning, (b) During welding, the position of the lap joint, (c) On the upper plate, lack of fusion throughout the joint line, (d) On the lower plate, no fusion, only deformation was observed

3. Processing on a Butt Joint

As seen in Fig. 48 (c), welding was processed at 1800 rpm, 100 mm/min on a butt joint. Two 4 mm thick plates were used. After processing, no fusion was observed, only edge burning and staple fiber deformation were occurred as seen in Fig. 48 (d).

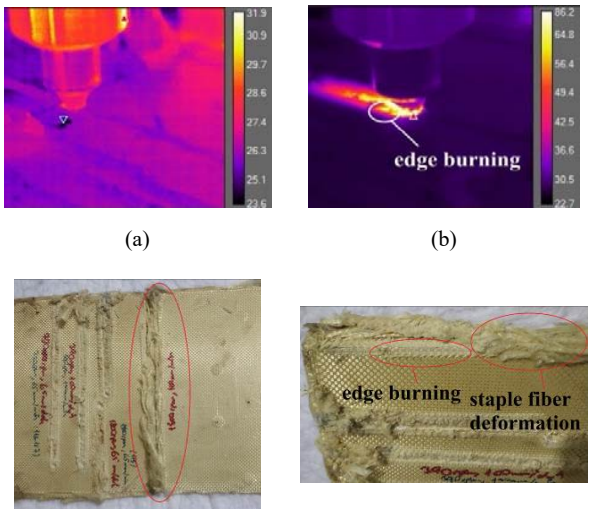

(a) (b)

(c) (d)

Fig. 48 Processing at 1800 rpm, 100 mm/min on a butt joint, welding was started at 32°C (a) and reached to max 86°C (b) in 11 seconds, (c) the welding image after processing, (d) no fusion, only edge burning and staple fiber deformation were observed

As seen in Fig. 49 (c), welding was processed at 720 rpm,

65 mm/min on a butt joint. Two 4 mm thick plates were used. After processing, no fusion was observed; only staple fiber deformation was occurred as seen in Fig. 49 (d).

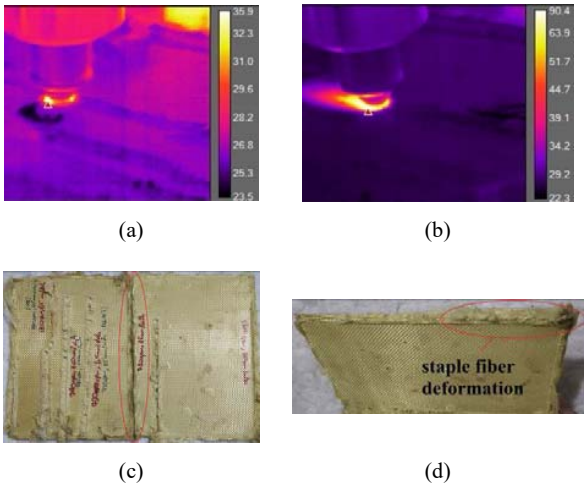

(a) (b)

(c) (d)

Fig. 49 Processing at 720 rpm, 65 mm/min on a butt joint, welding was started at 36°C, (a) And reached to max 90.4°C (b) in 41 seconds, (c) the welding image after processing, (d) no fusion, only staple fiber deformation was observed

Consequently, as seen in Fig. 50, Kevlar® material losses weight in large amount after 200°C [21]. Due to the weight loss from both the fiber and the resin- , the void volume of the composite increases and the shear stress is affected negatively because of this change. Aramid is very tough allowing significant energy absorption but, compared to carbon, it is lower in compressive strength and has poorer adhesion to the matrix. Twaron CT 736 PHF Kevlar® product contains phenolic resin and it chars when heated to temperature greater than 250°C. The thermal conductivity of the phenolic resin is 451 W/mK and it is too high compared to that of Kevlar® (0.04 W/mK).

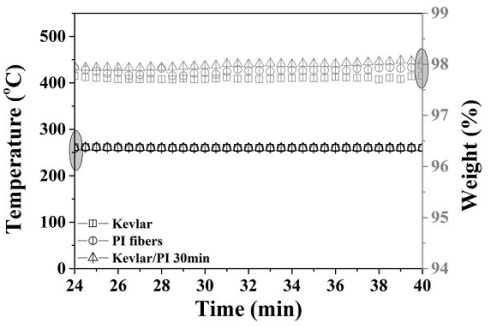

Fig. 50 The weight loss of Kevlar® as a function of time at elevated temperatures (isothermal step at 260°C)

Due to above results, during welding process, when heated to temperature greater than 250°C, many imperfections such as cluster pulp burning, lack of fusion, spatter and staple fiber deformation were observed.

VII. Conclusion

Thanks to its light weight, ability to absorb large impact energies and its good ballistic protection including stab and knife resistance, Kevlar® is a widely preferred material in aerospace and defense industry. According to the technical guide of Kevlar®, it neither burns nor melts, however, over long periods of time at elevated temperatures (exceeding 250°C), it can suffer degradation, which in this study, were observed in form of cluster and/or pulp burning, edge burning and spattering.

For the complex shapes designed by modern industries especially in automotive and aerospace industries, two or more layers of Kevlar® are needed to bond together. As a general rule, synthetic fabrics such as polyester, nylon or polyamide can be welded using electromagnetic waves, but Kevlar® cannot be welded with FSW and via using a tapered circular with 3 flats pin, as it does not melt and there is immediate weight reduction. It can be suggested that during the manufacturing process of Kevlar®, the thermal conductivity of the resin should be selected closer to Kevlar® and by this way, the resin could protect the fibers and keep them together during the welding process.

References

[1] K. Kumar, Satish V. Kailas, "The Role Of Friction Stir Welding Tool On Material Flow and Weld Formation", *Materials Science and Engineering* A 485 (2008) 367–37.
[2] The ESAB Way, Friction Stir Welding.
[3] Rajiv S. Mishra, "Center for Friction Stir Processing, University Of Missouri", Rolla Murray W. Mahoney, Rockwell Scientific Company B.
[4] Jeroen De Backer, Bert Verheyden, "Robotic Friction Stir Welding for Automotive and Aviation Applications".
[5] R. Rai, A.De, H. K. D. H. Bhadeshia and T. DebRoy, "Review: Friction stir Welding Tools".
[6] DPT Kevlar Technical Guide, Aramid Fiber.
[7] Rene Lohmann, Sales & Marketing Ballistics, Teijin Aramid GmbH, Techtextile Middle East Symposium, Dubai, 20 th February 2014.
[8] Kerem Altuğ GÜLER, "Uçak Yapımında Kullanılan Malzemeler Ve Özelliklerinin İncelenmesi (Bitirme Tezi)", Yıldız Teknik Üniversitesi Kimya-Metalurji Fakültesi Metalurji Ve Malzeme Mühendisliği Bölümü.
[9] Vijay Shivaji Gadakha, Kumar Adepu, "Heat Generation Model For Taper Cylindrical Pin Profile In FSW".
[10] Friction Stir Welding, Solved with COMSOL Multiphysics 4.1.
[11] Basil M. Darras, "Experimental And Analytical Study Of Friction Stir Processing, University of Kentucky".
[12] S. Cui, Z.W. Chen, J.D. Robson, "A Model Relating Tool Torque and It's Associated Power and Specific Energy To Rotation and Forward Speeds During Friction Stir Welding/Processing", Department of Mechanical and Manufacturing Engineering, AUT University, NZ.
[13] James,R.S. 1990. "Aluminum-Lithium Alloys", *Metal Handbook Tenth Edition*, Volume 2: Properties and Selection: "Nonferrous Alloys and Special-Purpose Materials", *ASM International: Metals Park*, OH.178-199.
[14] Hill,R. 1956, "The Mathematical Theory of Plasticity", Oxford at the Clarendon Press.
[15] M. A. Martinez, C. Navarro, R. CorteS, J. Rodriguez, V. Sanchez-Galvez, "Friction and Wear Behaviour of Kevlar Fabrics", Department of Materials Science, E. T. S, Ingenieros de Caminos, Canales y Puertos, Polytechnic University of Madrid, Ciudad Universitaria s/n, 28040 Madrid, Spain.
[16] B. Saha Roy, T. Medhi, S. C. Saha, "Material Flow Modeling in Friction Stir Welding of AA6061-T6 Alloy and Study of the Effect of Process Parameters", *World Academy of Science, Engineering and Technology International Journal of Materials and Metallurgical Engineering* Vol:9, No:6, 2015.

[17] Dr. Yong Gan, "Continuum Mechanics-Progress in Fundamentals and Engineering Applications".
[18] James E. Mark, "Polymer Data Handbook", University Of Cincinnati.
[19] Brett D. Sanborn, Tusit T. Weerasooriya, "Effect of Strain Rates and Pre-Twist on Tensile Strength of Kevlar KM2 Single Fiber", Oak Ridge Institute for Science and Education, Weapons and Materials Research Directorate, ARL.
[20] Wagner et al, "United States Patent Application Publication", Pub. No.: US 2006/0234572 A1.
[21] Diana Serbezeanu, Ana Maria Popa, Timea Stelzi, Ion Sava, Rene ´ M Rossi and Giuseppino Fortunato, "Preparation and characterization of thermally stable polyimide membranes by electrospinning for protective clothing applications".